UNIVERSITY OF CALIFORNIA,
IRVINE

Methodology for Analyzing Multi Propeller Aircraft Community Noise and Procedural Applications

THESIS

submitted in partial satisfaction of the requirements
for the degree of

MASTER OF SCIENCE

in Mechanical and Aerospace Engineering

by

Nathan Ho-Juin Yeung

Thesis Committee:

2022

TABLE OF CONTENTS

LIST OF FIGURES

LIST OF TABLES

ABSTRACT OF THE THESIS

Methodology for Analyzing Multi Propeller Aircraft Community Noise and Procedural Applications

By

Nathan Ho-Juin Yeung

Master of Science in Mechanical and Aerospace Engineering

University of California, Irvine, 2022

The following work presents, outlines, and demonstrates a methodology used to analyze the community noise of multi propeller aircraft as well noise of procedural applications. This methodology is capable of propeller performance analysis and design, aircraft source noise modeling, and source noise propagation over a community. Aircraft source noise modeling captures the noise generated from propeller and aircraft geometry at local operating conditions such as onset velocity and propeller RPM. Noise propagation captures changes in altitude, attitude, and propeller performance over distance or time as specified by a flight profile. Varying the flight profile allows changes in operating procedure to be modeled.

Propeller analysis and design is performed using a program called XROTOR, which employs blade-element momentum theory to evaluate the performance and properties of a specified propeller geometry. Propeller performance is used along with aircraft geometry to generate a suitable flight profile. Aircraft source noise analysis is done using NASA's Aircraft Noise Prediction Program (ANOPP2)'s Blade Element Acoustic Tool (ABEAT) which models the broadband and tonal noise of propellers. Finally, the aircraft source noise is propagated along a flight path to community noise observers using ANOPP2's internal modules.

The aircraft noise model was shown to be valid based on its consistency with experimental data conducted about a single rotor and motor. With the addition of corrections to account

for deviations from ideal test conditions, noise results were found to agree within 1 dB. Further applications were explored to demonstrate the model's capability to analyze the noise effects of parameters ranging from propeller blade geometry to the aircraft's flight procedure. Applications of this methodology are demonstrated though case studies and preliminary assessments of an example aircraft. A propeller design study modeled variations in propeller diameter and blade count. The source noise analysis found that reducing blade radius and increasing blade count resulted in a reduction of overall noise. These results align with existing research concluding that a reduction in tip mach number and activity factor lowered overall measured noise. The methodology's noise propagation capabilities are demonstrated by performing a preliminary assessment on a sub-scale Short Takeoff and Landing (STOL) aircraft in takeoff, cruise, and approach conditions. The aircraft's modeled source noise was propagated as component and total noise over a community to create area contours representing ground noise distribution. The methodology's procedural analysis capabilities were also presented by varying glide slope to create alternate flight procedures. The results indicate that in STOL flight applications, propeller noise is dominant during departure and cruise, and that changes in thrust and glide slope have strong effects on approach noise.

Chapter 1

Introduction

Short and Vertical Takeoff and Landing (STOL/VTOL) aircraft make up a burgeoning sector in aviation. Though not a new concept, advances in battery technology, distributed propulsion, and development of infrastructure and demand, have made electric multi propeller aircraft a popular focus [1]. One example is Urban Air Mobility (UAM) whose concept has long been proposed in solutions, such as air taxis, to ease congestion in population centers. Other applications include delivery services to urban and suburban areas. Nearly all these scenarios involve operating propeller or rotor blades in close proximity to areas of human habitation [2]. There is interest to design and operate both propeller and aircraft in ways that minimize disturbing frequencies and amplitudes of noise [3]. Propeller and aircraft flight profile noise must be analyzed in tandem, since propulsive properties dictate how an aircraft is flown. These problems motivate the creation of the following methodology which analyzes the noise of multi propeller aircraft in applications relating to community noise and noise attenuation through flight procedure variations. This framework ties flight profile to propeller performance and aircraft flight characteristics. These three parameters serve as inputs for the aircraft noise modeling and propagation portions of the methodology.

Aircraft noise, in the context of this framework, is described as unwanted sound that causes nuisance and disturbance. Noise can be produced from flow about the airframe

and control surfaces or by propulsion in the form of rotor, propeller, and engine noise [4]. This methodology will focus on aerodynamic noise in the context of airflow interaction with propellers. For many proposed and current VTOL/STOL aircraft, propeller and rotor lift systems are identified as the primary source of aerodynamic noise. This is especially the case when operating in high lift regimes, such as takeoff [5].

The amplitude of noise is commonly measured as a Sound Pressure Level (SPL), defined in a logarithmic decibel scale (dB) [6]. One metric used in this study is Sound Exposure Level (SEL), which measures sound exposure relative to a reference value [7]. The human perception of noise, however, depends on frequency, where certain frequency bands are perceived as louder than others. When modeling noise, it is often useful to apply a weighed scale on amplitude at certain frequencies. This study will use one such metric called A-weighted Overall Sound Pressure Level (OASPL) [8].

When performing noise modeling and analysis, it is necessary to break aerodynamic noise into its constituent forms. For propellers and rotors, these are broadband and tonal noise as described in Figure 1.1. Tonal noise is periodic and is associated with harmonics of the blade passage frequency (blade number x rotational frequency). For this methodology's modeling, tonal noise is created by loading and thickness noise. Loading noise is a function of torque and thrust, and is caused by the chord wise pressure distributions along the blade. Thickness noise is caused by mass displacement of the propeller blade sections as they rotate through air. Broadband noise is primarily caused by vortices, formed and shed from the propeller blade's trailing edges and blade tips. Additionally, if propellers are operated in disturbed flow, turbulent fluctuations can also contribute to broadband noise [5]. In rotor craft, broadband and tonal noise manifest as propeller-airframe interaction and propeller-propeller interaction noise. These can include blade wake interaction from aft rotors experiencing the vortices of forward propellers or destructive interference from phased tonal noise of opposite propellers [9]. Airframe noise and propeller-wake interactions are not considered in this study.

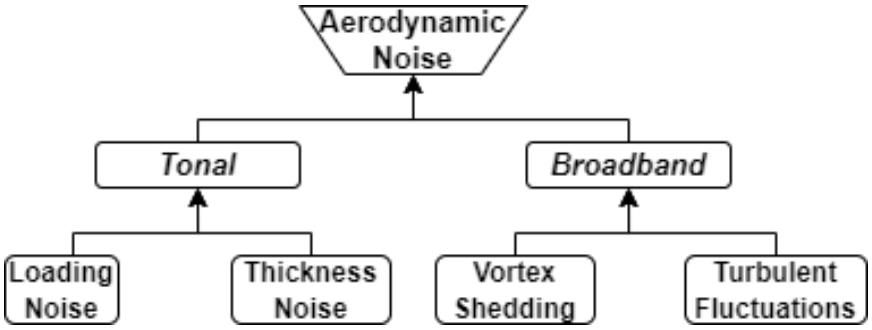

Figure 1.1: Types and sources of aerodynamic noise

A distinction must be made between source noise and community noise. Source noise is noise local to the aircraft. In the context of propellers, it is mainly caused by blade or rotor geometry and operating condition such as RPM and onset velocity. Community noise is taken with respect to a larger area on the ground. Figure 1.2 shows a hypothetical aircraft source hemisphere being flown on a flight path over a grid of community noise observers. Flight path parameters, such as altitude, attitude, and changes in RPM and speed, have a larger role in the noise characteristics produced. Because community noise is propagated from the a source, factors such as directivity also shape the magnitude of noise experienced at a point on the ground.

The community noise analysis methodology is described, validated, and its capabilities demonstrated in the following work. Chapter 2 breaks down the framework into three major modules of propeller performance, aircraft source noise, and community noise analysis. For each module, the theory behind each procedure is described, including their respective inputs, outputs, and suitable applications. Next, Chapter 3 compares the noise modeling capabilities of the framework against experimental data to validate the accuracy of the source noise generation and propagation modules. The propeller performance analysis and design capabilities are demonstrated with a case study in Chapter 4. Here, changes in propeller geometry are explored to optimize noise given performance parameters and operating constraints. Finally, a holistic case in Chapter 5 demonstrates aircraft community noise propagation and analysis. Here, the propeller performance analysis capabilities are paired

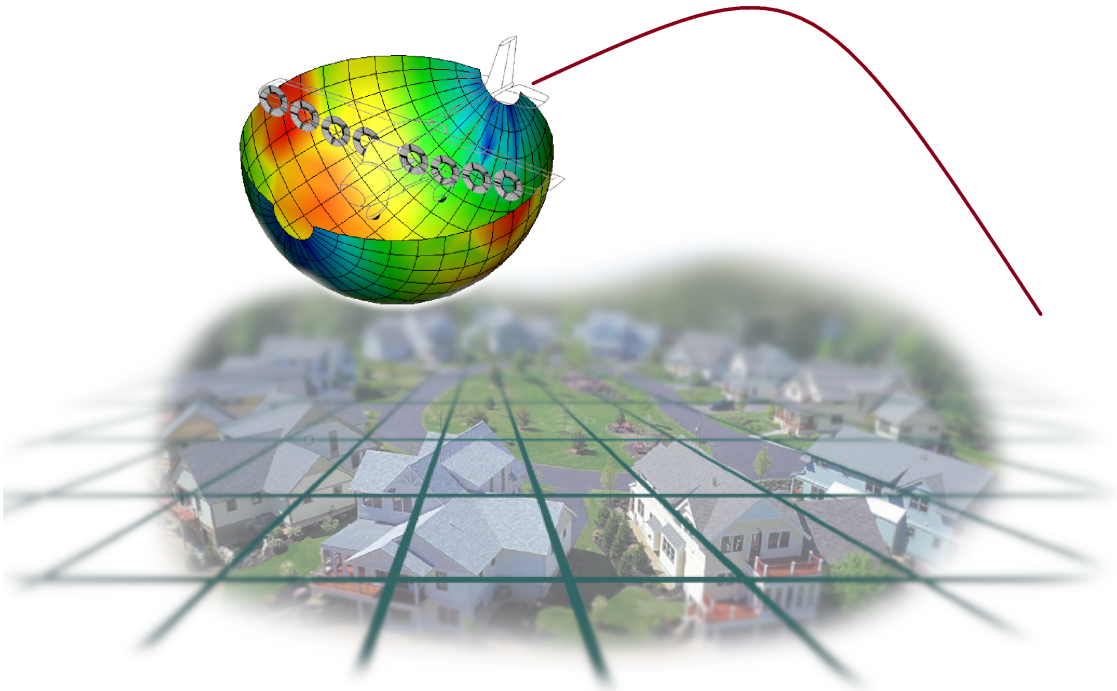

Figure 1.2: An example aircraft source noise hemisphere being propagated to a grid of community observers from the flight path highlighted in red

with existing aircraft data to explore the effects of alternate flight procedures on community noise.

Chapter 2

Model Framework

This methodology consists of three main modules: Propeller Performance Analysis, Aircraft Source Noise Analysis, and Noise Propagation based on a specified flight profile, as illustrated in Figure 2.1. A propeller of specified geometry is the input to both performance and noise analysis modules of the model. The resulting propeller performance data is used to create an aircraft flight profile, which then dictates operating conditions during the aircraft source noise analysis. Conversely, desired performance can be specified and a suitable propeller geometry can be generated and inputted into the aircraft noise analysis model. The ability to design also allows existing propellers to be modified to determine potential noise effects of certain elements. Once propeller geometries are imported in the noise analysis program, they are assembled to form a multi propeller vehicle based on specified aircraft geometry. A source noise hemisphere is then created based on the resulting broadband and tonal noise. This source noise hemisphere is based on local properties such as onset velocity, RPM, blade pitch, and phase angle, which are functions of flight profile. Finally, community noise is analyzed by propagating this source hemisphere to a grid of observers. Factors such as aircraft attitude, altitude, and propeller thrust are also specified by the flight profile. Here, directional factors, such as altitude and glide slope, can vary as a function of time. These capabilities allow this methodology to evaluate both local changes in propeller geometry and

power, as well as large scale variations in how the aircraft is flown over a community.

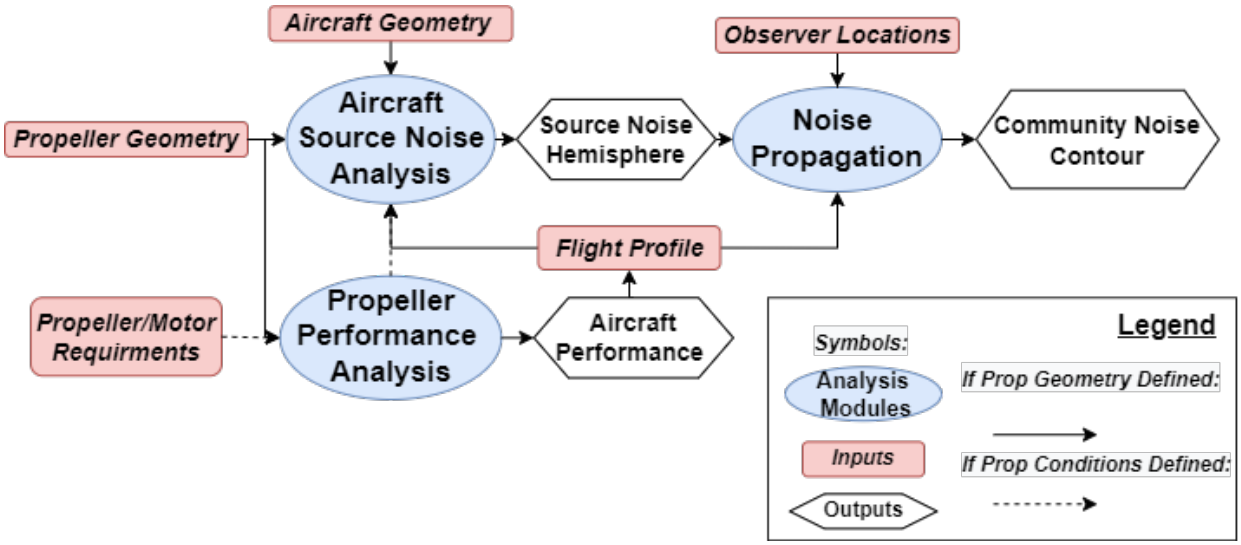

Figure 2.1: Methodology for Analyzing Multi Rotor Vehicle Community Noise and Procedural Applications

2.1 Propeller Performance and Geometry Generation

The goal of this subsection is to derive propulsion properties—such as thrust—at various air-speeds and power levels, which are later used to compute the vehicle flight profile. If geometries are unknown, motor performance and desired propulsive properties are used to design the propeller blades, which then become inputs to the noise module. Propeller performance analysis and design is done using an interactive program called XROTOR [10], which is based on classical blade-element and vortex theory solidified by Betz, Goldstein, and Theodorsen [11] [12] [13]. The program uses augmented blade-element theory to provide a more accurate analysis for heavy disk loading and more consistent design and analysis results [10]. The methodology's design and analysis capabilities allow it to capture effects of detailed blade and propeller geometry changes on overall aircraft noise.

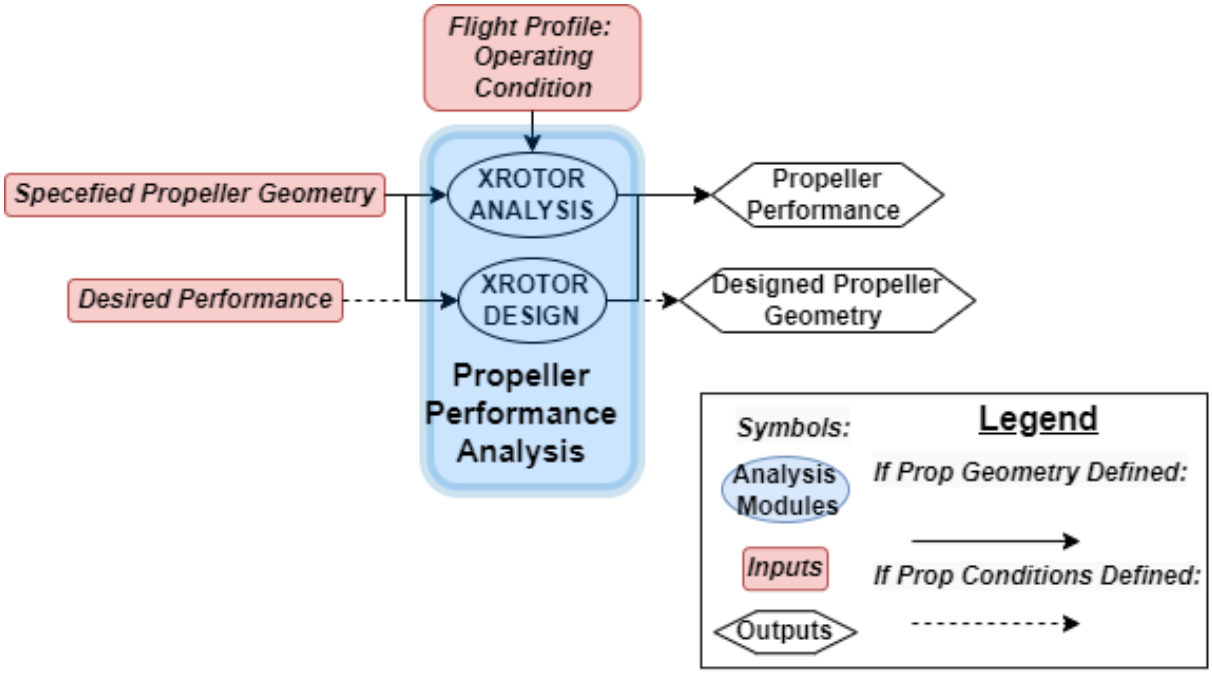

Figure 2.2: Framework of the Propeller Performance Analysis and Design Module

2.1.1 Propeller Performance Analysis Module

If propeller geometry is specified, the framework models propulsion properties at various airspeeds, density altitudes, and operational points such as RPM. The propeller geometry input includes chord distribution $c(r)$, blade twist distribution $\beta(r)$, and overall parameters such as blade count and propeller radius. Performance outputs include thrust, power, and torque. This analysis ensures the required vehicle thrust is achievable with a given propeller design. Additionally, off-design operational conditions can be analyzed, such as varying RPM and airspeed for a given design. These design points are used to pair flight path properties—such as glide slope—to their corresponding propeller power level. The resulting parameters are used to create a flight profile which will later be inputted to both the Aircraft Source Noise Analysis module and the Noise Propagation module.

For this purpose, XROTOR was selected because of its ability to vary desired parameters, and for its closeness in matching propeller performance analysis with design. The following description comes from theory documentation describing the formulation of XROTOR [10].

The program starts by decomposing relative velocity and adding a tangential "swirl" velocity caused by the torque of the propeller blade. Prandtl's tip loss factor is modified by using the blades local wake advance ratio, λ_w rather than the rotor's average ratio because this provides a more accurate result for heavy disk loading. The local angle of attack is based on the geometric twist angle, β, and the local decomposed velocity. This is also used to obtain the section blade circulation, Γ. Finally, the radial circulation distribution, $\Gamma(r)$, is calculated independently at each section using blade rotation, velocity, $c(r)$, airfoil section information, c_d and c_l, and $\beta(r)$. Newton's method is used to iterate the residual as a function of c_l and Γ. Propeller thrust and torque are analyzed by integrating the radial $\Gamma(r)$.

2.1.2 Propeller Design

Conversely, if blade geometry is not specified, a propeller capable of meeting desired aircraft performance is created. Blade chord and twist distribution are generated for a given propeller diameter, blade count, RPM, power, and airspeed. Other details, if known, can also be specified, such as c_l distribution, advance ratio, torque, and desired thrust. This portion of the framework also has the capability to modify existing geometry. Rotor diameter can grow or shrink, blades can be re-twisted, their chords can be re-shaped, and number of blades reduced or increased. These changes can all be done while preserving either power, thrust, or RPM. Similar to the steps in Section 2.1.1, the performance data is used to create a flight profile. This and the resulting propeller geometry are inputted to the Aircraft Source Noise Analysis module.

Blade design is functionally identical to the analysis portion, except, thrust, torque, or an RPM/torque relation must be specified. $\beta(r)$ and or c_r will be treated as unknowns and Newton's residual will be parameterized as a function of V, Ω, β, c, and a final variable representing propeller loading. This is set by specifying either thrust or torque. Ultimately, the main propeller design prerogative is to create geometries resulting in Minimum Induced Losses (MIL), constant radial efficiencies, and the maximum induced efficiency for its operat-

ing condition [10]. For the Aircraft Source Noise module, the relevant result is a distribution of $c(r)$ and $\beta(r)$ that is used to generate a 3-D propeller. The use of XROTOR allows creation and noise analysis of blade count, solidity, thrust, RPM, and motor power.

2.2 Aircraft Noise Analysis Module

For this, NASA's ANOPP2's Blade Element Acoustic Tool (ABEAT) [14] was used to model vehicle propeller noise. Functional modules exist within the program to model the propeller blade, calculate rotor loads, and calculate broadband and tonal noise created during the propeller operation as shown in Figure 2.3. For a specific vehicle model, modules are selected to allow unique configurations of propeller geometries and operation conditions which permit a wide breadth of multi rotor and propeller vehicles to be considered. The program has numerous user defined parameters such as tip loss conditions and multiple inflow models. Noise outputs can also be expressed in various types of sound pressure levels such as A-weighted Overall Sound Pressure Level (OASPL).

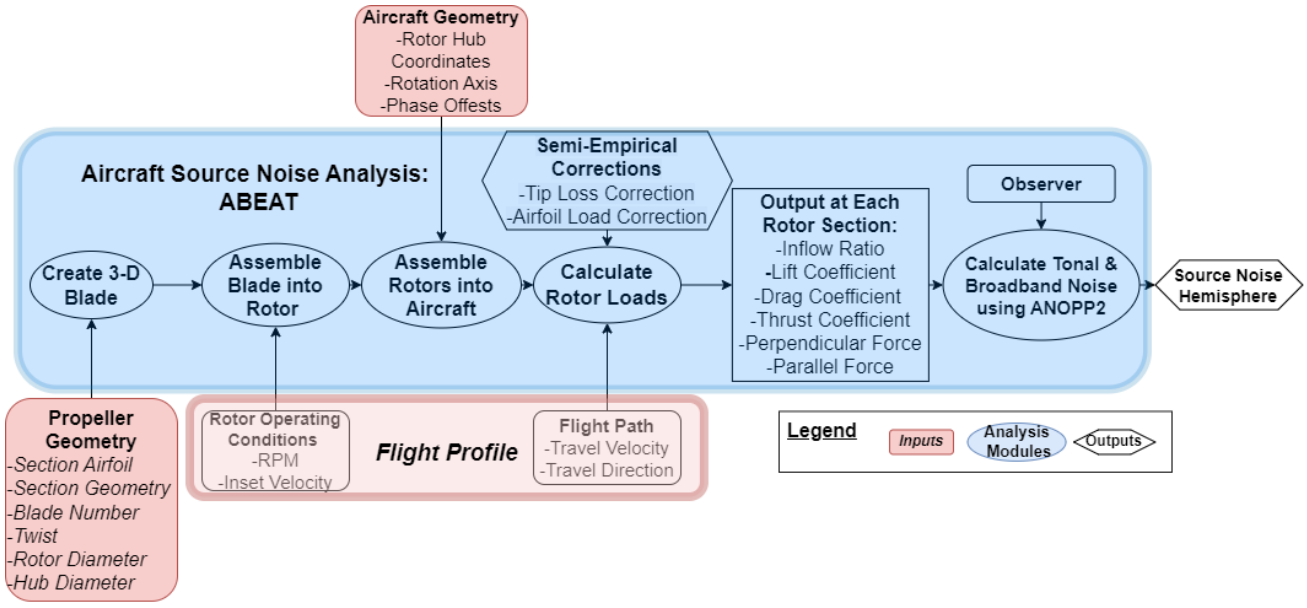

Figure 2.3: Framework of the Aircraft Source Noise Modeling and Analysis Module.

A vehicle is constructed based on the previously defined blade geometry and the spacial

propeller positions which are specified by the aircraft geometry input. Parameters such as propeller phase and rotor plane tilt angle are specified according to vehicle configuration. The resulting vehicle noise is then modeled based off the pressure distribution and rotor loads at the RPM and onset velocities provided by the flight profile. Propeller noise analysis employs classical blade-element momentum theory to model blades as lifting lines. From here, tonal noise is calculated from blade thickness and the Ffowcs Williams and Hawkings equation using Farassat Solution 1A [15]. Broadband noise resulting from turbulent blade interactions are calculated using semi-empirical methods [16]. From here noise levels are recorded using observers spaced around the vehicle to create a source hemisphere which later propagated to create a community noise profile.

2.2.1 Propeller Surface Modeling

Specified propeller geometry is used to create lifting-line models of the blade. This is done by dividing each blade into radial sections, r/R. Each radial division then specifies $c(r)$, local airfoil data, $\beta(r)$, leading and trailing edge radii, trailing edge thickness, and leading edge ordinate and abscissa points. The last parameter defines each section's position in space. Other geometry, such as rake and skew, would be specified by shifting each section's ordinate position. Hub diameter is also specified by omitting data within the innermost radial station. Higher model density is desired around areas of greater geometric change such as the propeller tip [17]. The result is a mesh grid surface model of each propeller blade. An example is illustrated below in Fig 2.4.

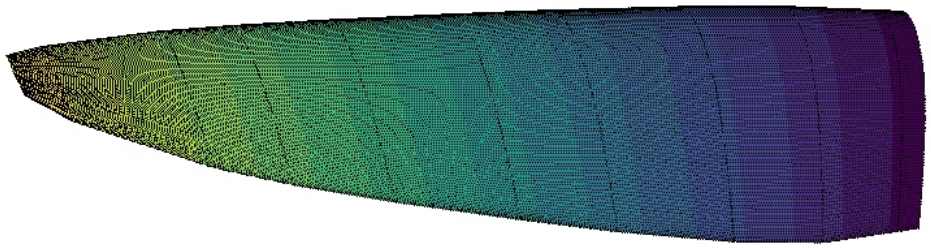

Figure 2.4: Mesh surface model of the propeller blade

The single blade is then patterned symmetrically about the e_θ rotation axis in the propeller coordinate system, (e_r, e_θ, e_ϕ) as defined in Figure 2.5. This results in a single, complete propeller. Rotation direction is then specified and blade geometry is inverted as necessary to produced either left or right "handed" propellers. Phase offset is also specified at this point, which allows the model to capture in and out of phase propeller operation. Lastly, the propeller tilt angle is specified for each rotor with respect to the local onset velocity. Dictated about the e_ϕ axis, this parameter allows the framework to model setups ranging from conventional fixed wing to VTOL tiltrotor applications. The previous modeling steps are repeated for each subsequent propeller.

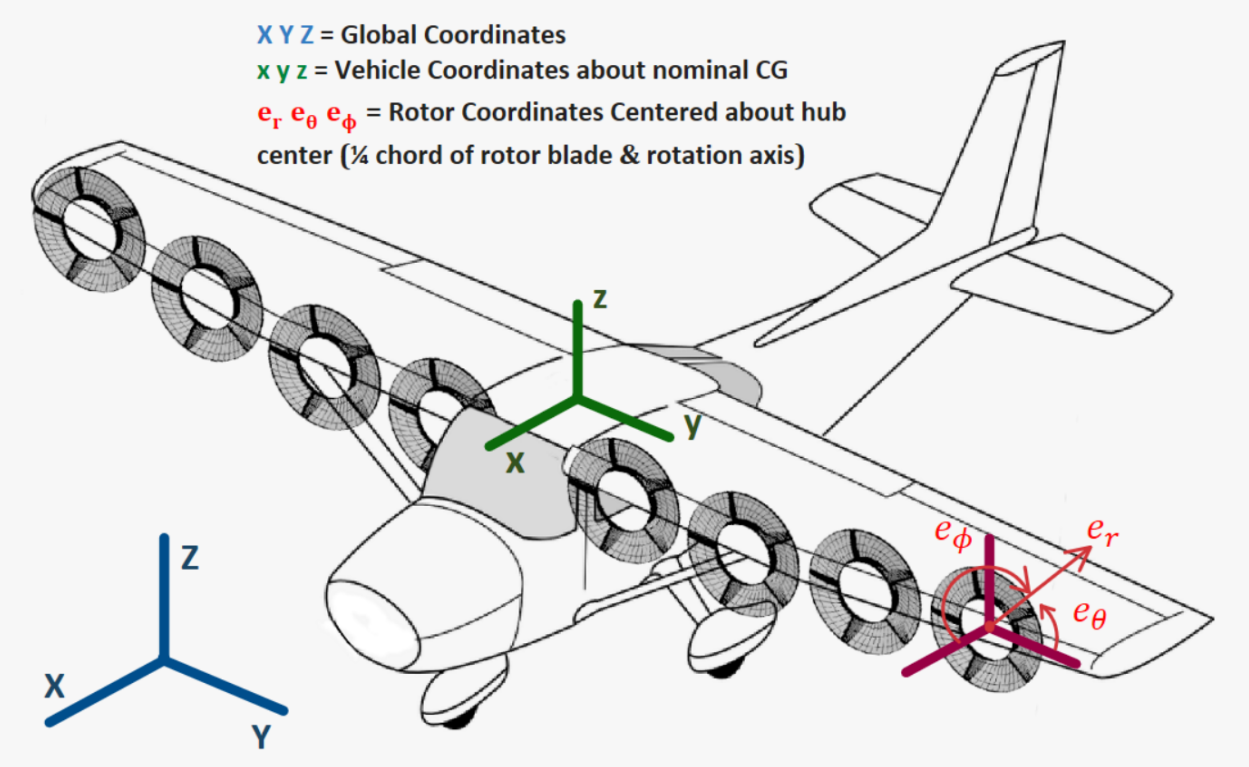

Figure 2.5: Definition of propeller, aircraft, and fixed coordinate systems

Once propellers of correct geometry, phase, and local orientation are defined, they are combined into a single vehicle using the aircraft geometry input. The propeller locations are specified with respect to the vehicle coordinate system, (x, y, z). An example aircraft with different propeller diameters, rotation direction, and phase angle is shown in Fig 2.6.

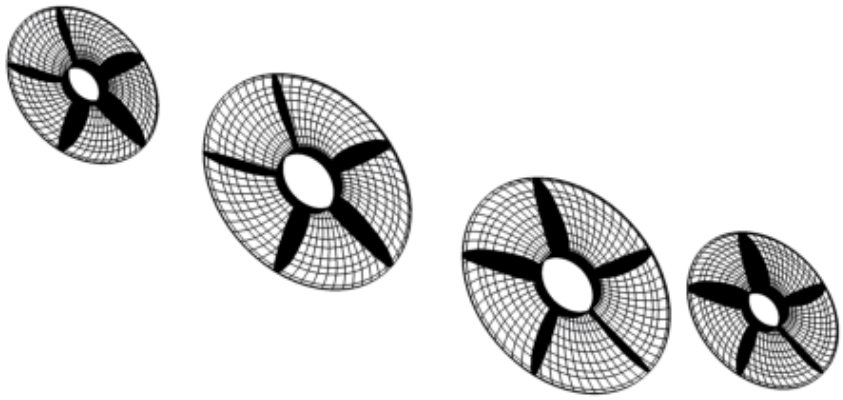

Figure 2.6: Example of a modeled multi rotor aircraft with counter-rotating multi diameter propellers

2.2.2 Rotor Load Calculation and Inflow Modeling

Once a vehicle has been defined, it is "flown" at an onset velocity defined by the flight profile. This velocity is a function of thrust and aircraft lift, and is specified with respect to the ground coordinate system, (X, Y, Z), described in Figure 2.5. Propeller loads are calculated in an iterative process based on the inflow model, section c_l and c_d, thrust coefficients, and rotor thrust. Propeller loading calculations are largely based on classical blade-element theory inflow, which iterates c_l, c_d, and thrust until the results converge [18]. The following section documents inflow models specified to suit possible model applications.

The basic solution of actuator disk momentum theory, as presented in Leishman's *Principles of Helicopter Aerodynamics*, works well for static cases and hover [19]:

$$\lambda = \mu tan\alpha + \frac{C_\tau}{2\sqrt{\mu^2 + \lambda^2}}$$

A more accurate inflow model, however, is based upon Glauert's departure from pure blade-element theory, which better accounts for the down-wash and up-wash on the leading and trailing edge of the propeller blade [20]:

$$\lambda = \lambda_0(1 + K_c r cos(\phi) + K_s r sin(\phi))$$

Here K_c and K_s are weights that act as deviations from the uniform inflow of momentum theory. Experimentally derived values for advancing propellers—such as in a VTOL applications—would prefer greater inflow towards the rear of the rotor. Shaped wakes can also be created in the model. Coleman et al., developed an analytical model used to create a cylindrical wake model and defines K_c as follows [21]:

$$K_c = tan(\frac{x}{2})$$

These non-uniform inflow expressions are useful to model fluctuations in pressure distributions. Using the desired inflow model, the radial blade lift, drag, and thrust coefficients are calculated. The resulting forces are decomposed into their respective perpendicular and

parallel components. These are also used to model other parameters such as pressure distribution on the blade surface. The outlined methodology will focus on uniform inflow models, since all propellers examined in the study operate in undisturbed airflow.

2.2.3 Source Noise Analysis and Generation

Propeller noise is modeled based on the resulting rotor load forces. Tonal noise is modeled by solving the Ffowcs Williams-Hawkings Equations (FW-H), which are time dependent harmonic wave acoustic analogies. They are functions of density, surface velocity, and pressure distribution [22]. Formulation 1A of Farrassat (F1A) is one solution found to have excellent utility for helicopters and propeller-based vehicles operating at subsonic speeds [3]. This formulation is based off solving the Thickness Noise and Loading Noise equations of FW-H imposed on a moving surface [15]. By ignoring the quadrupole source terms, F1A is able to represent FW-H as an integral function to avoid the need for computationally complex CFD methods [3]. The use of isometric translations also make Formation 1A particularly convenient for aeroacoustic applications because distances to both moving and stationary observers are preserved [23]. For this step, the framework employs an ANOPP2 internal module which implements 1A over the moving surfaces of the modeled propeller blade.

Broadband noise is calculated semi-empirically due to the unsteady fluctuations resulting from turbulent flow. The methods used in this framework is based off the Brooks, Pope, and Marcolini model (BPM) [16] of calculating airfoil self-noise. This model identifies and accounts for self noise due to trailing edge boundary layer turbulence, laminar boundary layer instabilities, trailing edge vortex shedding, and turbulent vortex flow about the blade tips [16]. Originally developed for airfoils in steady flow, the BPM model has been adapted for use in rotors using a quasi-steady state assumption around each blade section [24]. Noise predictions are then done by taking the mean square pressure along the rotor radius [25]. For this, an ANOPP2 internal functional module was used to implement the BPM method.

The broadband and tonal noise results are used to create the aircraft source noise output

though the use of local observers. Depending on the application, observer geometry can range from a two dimensional ring, to a full 3-D hemisphere as shown in Figure 2.7.

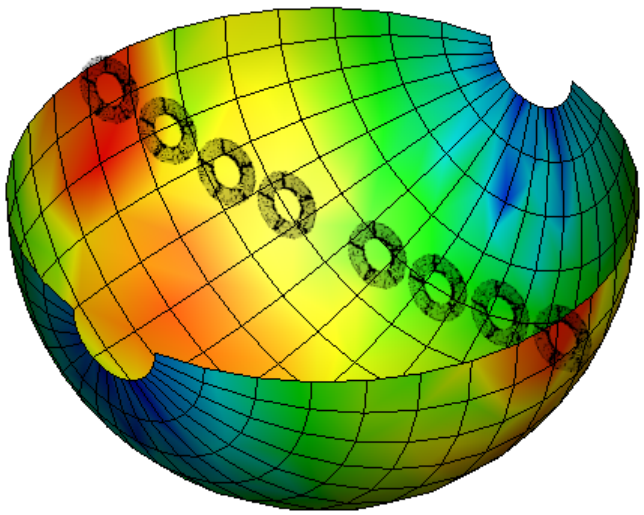

Figure 2.7: Example vehicle model and aircraft source noise hemisphere

2.3 Noise Propagation Module

Once the vehicle source hemisphere is created, it can then be propagated to noise observers over a specified area. This procedure is based on straight ray modeling, which assumes noise from a source is primarily transmitted along a direct path and a reflected path to an observer [26]. Atmospheric conditions that would curve a noise path, such as wind and temperature variations are not considered in the scope of this study. Noise attenuation and diffusion effects are modeled using specified atmospheric properties [27].

Noise propagation requires the vehicle's local flight path, global position, angles of attack, and attitude relative to local wind. Noise levels in the source hemisphere are also allowed to vary with position. This is specified though a flight path, which allows forward velocity, altitude, and RPM to be changed as a function of time. This enables the framework to associate propeller performance to flight angles, which is used during noise propagation. Possible noise propagation results include proportional band spectrum (PBS), narrow band spectrum (NBS), power spectral density spectrum (PSD), and overall sound pressure level

(OASPL).

The resulting spherical source noise propagation is then recorded with community noise observers. Placed along the ground trajectory of the aircraft, these record a ground noise contour as the aircraft follows its specified flight profile. The flight profile dictates altitude and attitude as a function of distance. The aircraft source noise analysis of Section 2.2 generated aircraft noise under constant conditions. These steps, however, can be repeated as the aircraft propellers operate in different regimes. The subsequently generated source noise hemispheres are propagated according to the flight profile. These flight profiles include forward velocity, RPM, blade pitch, and even propeller tilt angle.

Chapter 3

Propeller Model Data Validation

The results of propeller noise modeling methodology, described in 2.2.3, was experimentally validated against recorded sound data. To do so, the noise levels of a propeller with known geometry and operating conditions were measured and compared to the results when modeled in the exact same conditions.

3.1 Stationary Propeller Experiment

The acoustic experiment was conducted around a ground-mounted, static 5-bladed propeller and motor. The motor was fixed with its shaft horizontal such that the propeller's axis of rotation was parallel to the ground. Nine microphones were radially spaced to form a half-circle running from fore to aft of the propeller at the same height as the motor shaft. This is illustrated in the isometric view below in Figure 3.1, where the microphones are represented as ellipses. The noise testing was run at three different RPM's, each differing by 1000 RPM between each case. At each RPM the A-weighted sound pressure level was recorded using the nine hub-height microphones (model SRTW-mk3 from Convergence Instruments).

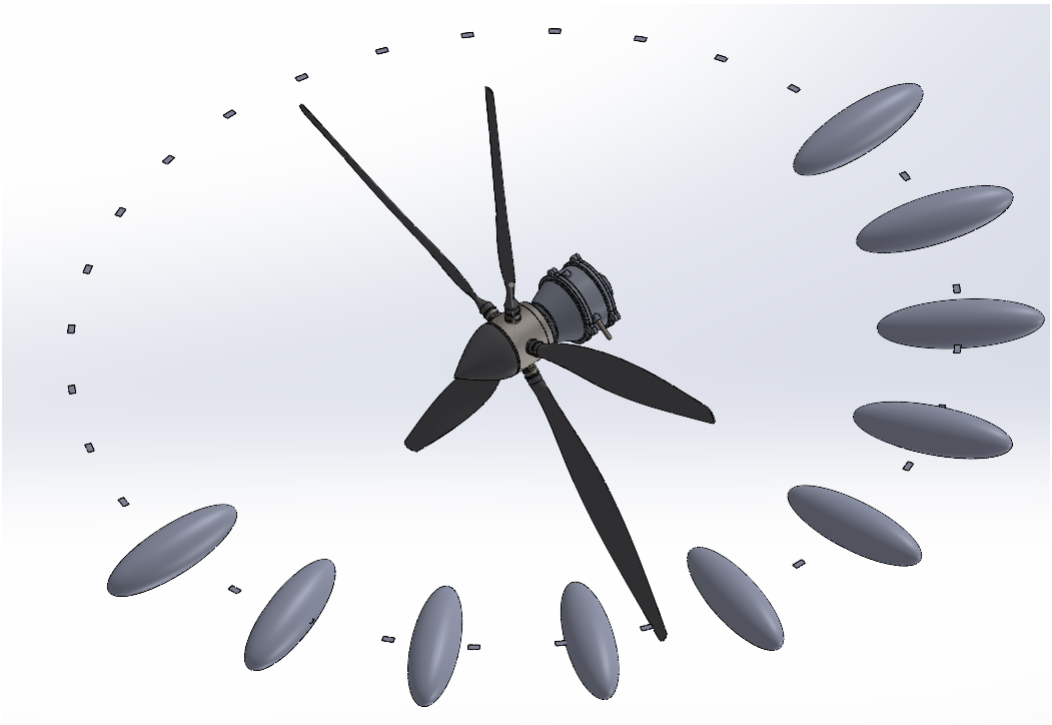

Figure 3.1: Model of the propeller, motor, and microphones which are represented as ellipses

This orientation was intended to record the variations in noise forward to aft of the propeller. Due to the radial symmetry of the propeller and motor, this setup allowed a semi-spherical noise distribution to be recorded with a small number of microphones positioned in only one plane. Finally, the noise of the motor alone was recorded at the same discrete RPM levels. This was to allow its noise to be subtracted from the overall measurements so that the propeller noise could be isolated in magnitude.

3.2 Stationary Propeller Model

The noise levels of this propeller were modeled by the module described in Section 2.2, using the previously described RPM levels. Nine noise observers were placed equally spaced in a semicircle of the same radius as the experimental microphone setup. The modeled propeller was centered about this half ring of observers. This was to ensure close similarity to the operating conditions and microphone placement as observed by the experiment. Broadband

and tonal noise were calculated assuming a uniform inflow model and an inset velocity of zero to simulate a static propeller operation. Finally, to provide more comparable modeled results with that of the experiment, isolated motor noise and ground reflection corrections, described in Section 2.3, were added to the modeled output.

3.3 Results

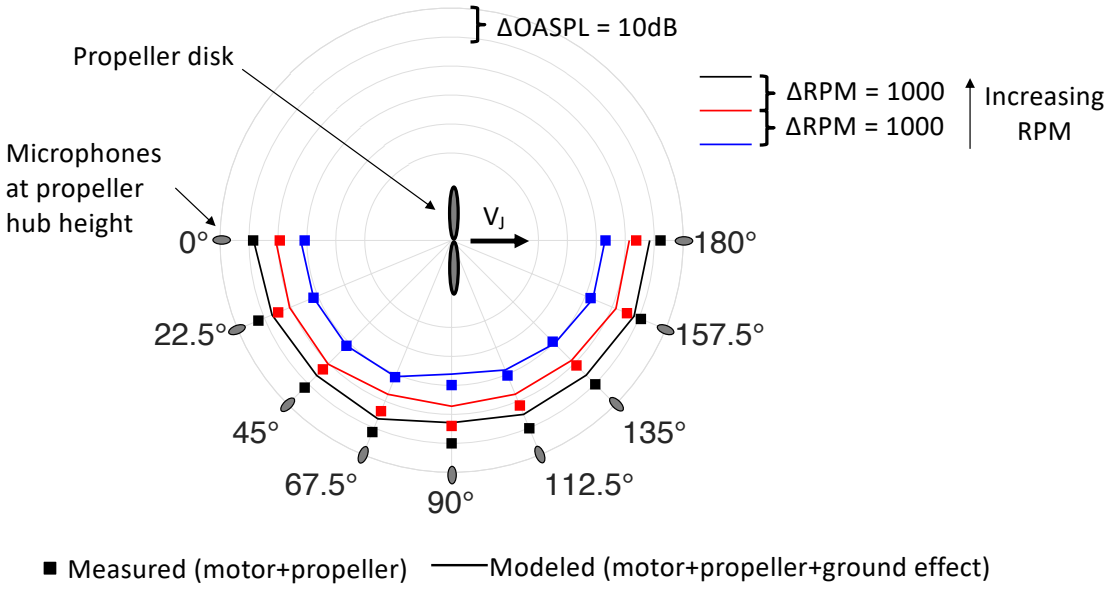

Figure 3.2: Measured and modeled static 5-bladed propeller noise levels at varied RPM settings

The noise model results with motor noise and ground effect corrections added are shown as continuous curves in Figure 3.2. Test noise levels, measured by the microphones, are depicted as discrete points. Close agreement between modeled and experimental noise levels were observed towards the forward and aft positions of the propeller across all operating RPMs, with certain points agreeing to within 1 dB. Low RPM cases matched very closely across all microphone stations while higher RPM cases diverged slightly on the sides of the propeller. The higher discrepancies around the 90° position were likely caused by noise reflections and other interactions with a hard safety barrier that was placed in the propeller

plane during the propeller testing. Other possible explanations for the disagreement in noise include additional reflections from the hard ground below the rotor. Otherwise, the results indicated sufficient model result agreement for initial validation of the Aircraft Noise Analysis module.

Chapter 4

Case Study: Rotor Design Application

The following case study demonstrates how the propeller design and noise prediction portions of the framework can be utilized in propeller design. Here, it is used to redesign an existing propeller, down-select different geometric features, and optimize multiple propeller geometries to minimize noise while retaining desired levels of performance. These factors include blade count, blade radius, $\beta(r)$, and $c(r)$. Potential contributors of noise were hypothesised to involve tip mach number and rotor solidity. These parameters were varied to observe changes in noise when a given propeller design was operated in off-design conditions. Torque, RPM, and power limits were set by motor design, and the required thrust was specified by the vehicle's climb and takeoff requirements.

4.1 Candidate Propellers Design Procedure

Several candidate propellers were created to test the effects of rotor diameter and blade count on propeller noise and performance. They were designed based on the performance parameters of a multi propeller aircraft with known propeller geometry. Since takeoff performance was prioritized, the design velocity for all propellers was chosen to be closer to takeoff

speed. For each candidate selection, $\beta(r)$ and $c(r)$ were re-distributed as either propeller diameter or blade count was altered in the process described in Section 2.1 of the framework. Maximizing thrust was an important criteria for this specific design study. Each candidate propeller was designed to operate under maximum motor power, which was limited to either maximum RPM or peak torque—whichever parameter was reached first. The optimization criteria was to shape and twist the blades such that the MIL condition, described in 2.1.2, was met. This was to ensure that geometric changes were compared fairly, as a single blade design would not be expected to operate efficiently if it were simply scaled up in radius or blade count.

4.1.1 Propeller Diameter Candidate Design

For the blade radius study, three different blade diameters were selected: radius A (RA), radius B (RB), and radius C (RC). These are shown as profile views in Figures 4.1a, 4.1b, and 4.1c. The radius was increased by 2 inches between RA and RB and between RB and RC. Blades were shaped and twisted in the Propeller Design Module to meet the MIL criteria. For all propellers, hub size, advance ratio, and c_l distribution were held constant so that each candidate propeller could be comparable to the aircraft's current design.

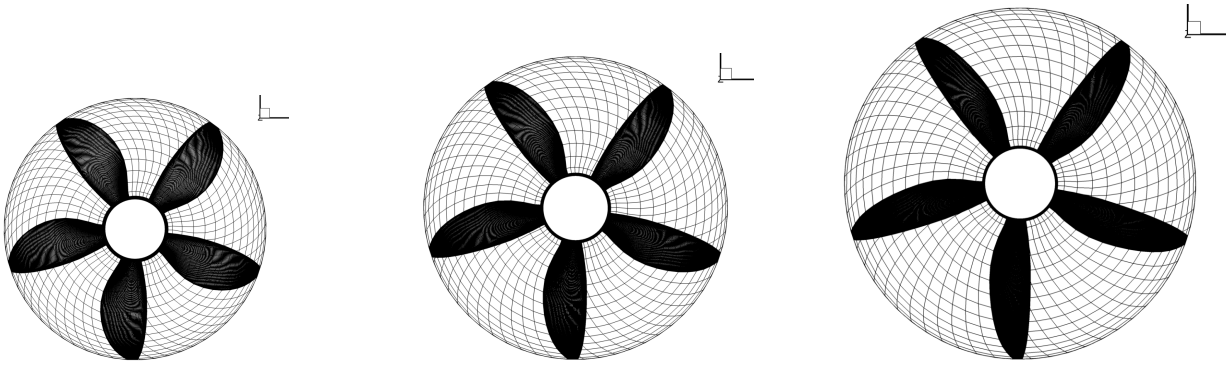

(a) 5-Bladed Propeller of Radius A

(b) 5-Bladed Propeller of Radius B

(c) 5-Bladed Propeller of Radius C

Figure 4.1: Candidate propellers for diameter change study

For the blade count study, a 7-bladed propeller of radius A (RA-7) was created. Blade count effects were evaluated by using the 5-bladed RA as a baseline case in which both share the same diameter. Propeller RA is shown alongside RA-7 in Figure 4.2b.

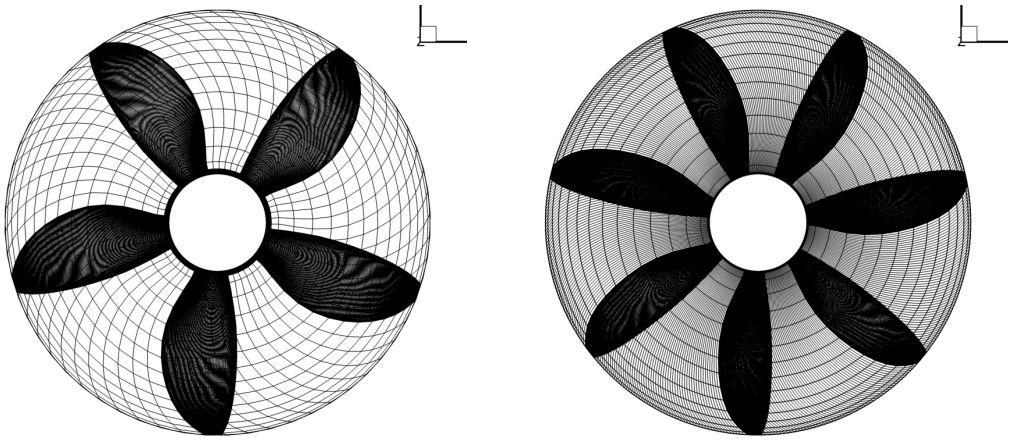

(a) 5-Bladed Propeller of Radius A (b) 7-Bladed Propeller of Radius A

Figure 4.2: 7-bladed candidate propeller, RA-7, compared to RA

The overall design philosophy was to ensure changes in geometry were implemented in an optimized and realistic way. For this reason, thrust, at optimal design conditions, was permitted to change as a smaller diameter propeller would not be expected to produce the same thrust as its larger variant given the same motor power. Additionally, a low design flight speed was chosen to approximate the vehicles takeoff conditions.

4.2 Propellers Modeling and Noise Analysis Procedure

Each of the three candidate propellers were modeled as described by the framework in Section 2.2. Individual blades were inputted to the program based on the propeller design geometry output and assembled into a propeller. Vehicle noise was not of interest in the current study so the rotor loads were calculated for a single propeller flown at a constant velocity. The 5-laded propellers of RA, RB, and RC along with the 7-bladed propeller, RA-7, were run at a constant RPM and onset velocity. The modeled velocity was that of vehicle's takeoff segment

where such high thrust would be necessary. Modeling only a single propeller also allowed the use of a considerably simpler uniform inflow model when calculating rotor loads since the propeller plane is normal to the onset velocity. These loads were then used to generate tonal and broadband noises using the framework described in 2.2.3. Noise results were then recorded by a half-circle of Nine observers in a similar fashion to the noise validation setup illustrated in Figure 3.2. This was possible due to the single propeller setup, in the absence of a full vehicle. The radius of observers was set to be five times that of the propeller so that far field noise characteristics can be adequately captured. The result of this aircraft propeller and propagation analysis are a set of tonal NBS and broadband PBS noise values. These are used to calculate total noise, which is expressed as an A-weighted OASPL.

4.3 Case Study Results

4.3.1 Effects of Diameter

The results of the diameter study are presented in Figure 4.3. The propeller is oriented with its axis of rotation parallel along the $0 - 180°$ axis. Each radial division represents a noise magnitude change of 5 dB. Propeller RA had the lowest noise contour, having almost a 5 dB difference from RB at stations $0°$ and $180°$. The change in magnitude lessened as the observer stations approached the propeller tip. Propellers RB and RC showed similar changes in noise with RC having a louder contour, but at a lesser increase of around 1 dB. All three propellers shared the same characteristics concerning directivity, with total noise being loudest at the tip.

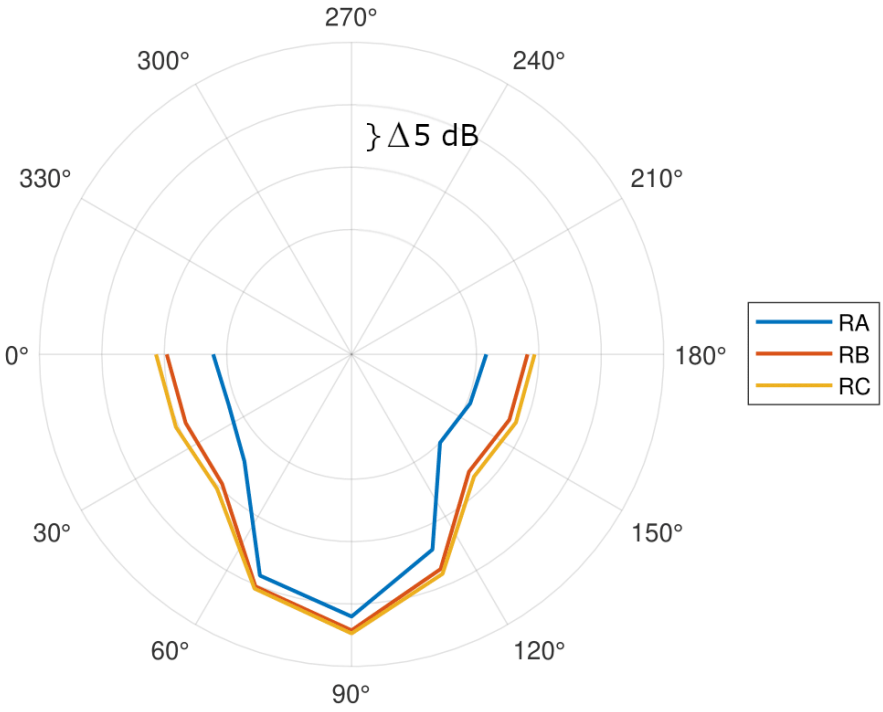

Figure 4.3: OASPL Noise contour (dB) for propeller radii A, B, and C

These results align with previous research concluding that for the same power, a change in propeller diameter had the effect of altering tip speed and radial loading. Decreasing diameter lowers tip speed but increases blade loading, because a smaller diameter propeller has to absorb the same motor power [17]. Since the modeled propellers operate under the same RPM, blade diameter is directly related to tip speed. Although increased rotor loading was found to increase propeller noise, the percentage of change was less than the effect of increasing RPM [28]. When experimentally tested, these noise reducing effects counteracted noise increases caused by the greater disk loading [5].

The modeled results also agreed with analytical predictions of noise. Hicks and Hubbard developed a semi-empirical method of propeller vortex noise along the trailing edges and tips. Their expression suggested that tip vortex noise could be reduced by minimizing tip velocity. Against experimental data, they found that vortex noise strongly correlated to tip velocity, finding that in some cases, doubling blade velocity increased SPL by 18 dB [29]. These trends are shared by the modeled results shown in Figure 4.4, which reveal significant

increases in average noise as the propeller tip Mach number increased from .45 to .50 across propellers RA, RB, and RC.

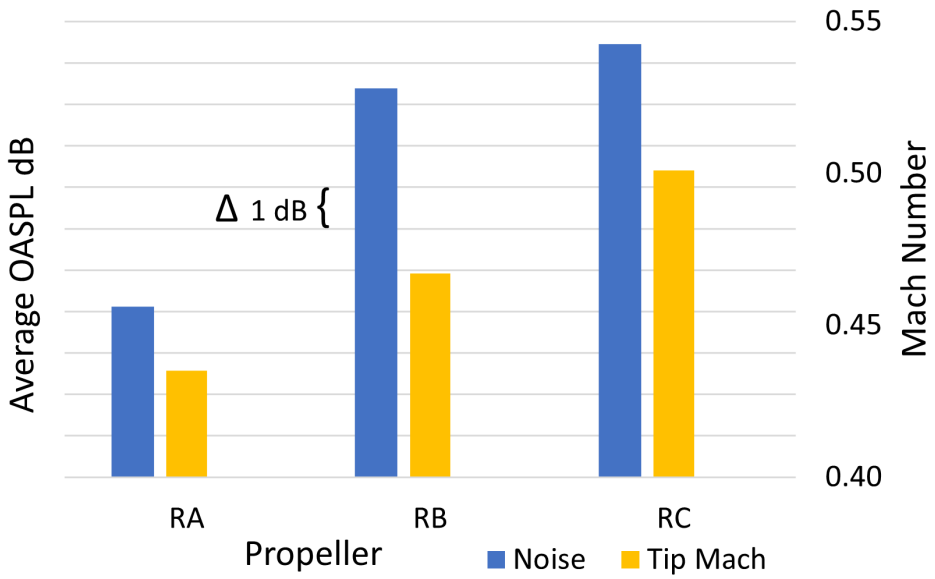

Figure 4.4: Change in average OASPL (dB) compared to Mach number at the propeller tip for radii A, B, and C

4.3.2 Effects of Blade Count

Propeller RA-7 was modeled under the same conditions as described in the cases above and the results are shown in Figure 4.5. The 7-bladed RA-7 was nearly 10 dB quieter at the tip observer compared to its 5-bladed counterpart. The strong directivity patterns towards the tips, however, was not as pronounced for RA-7 as compared to cases RA-RC. Towards the front and rear of the propeller, along monitors 0°–30 and 150°–180° respectively, RA-7 was 1-2 dB louder. Overall, the 7-bladed propeller was on average almost 5 dB quieter than its 5-bladed base design.

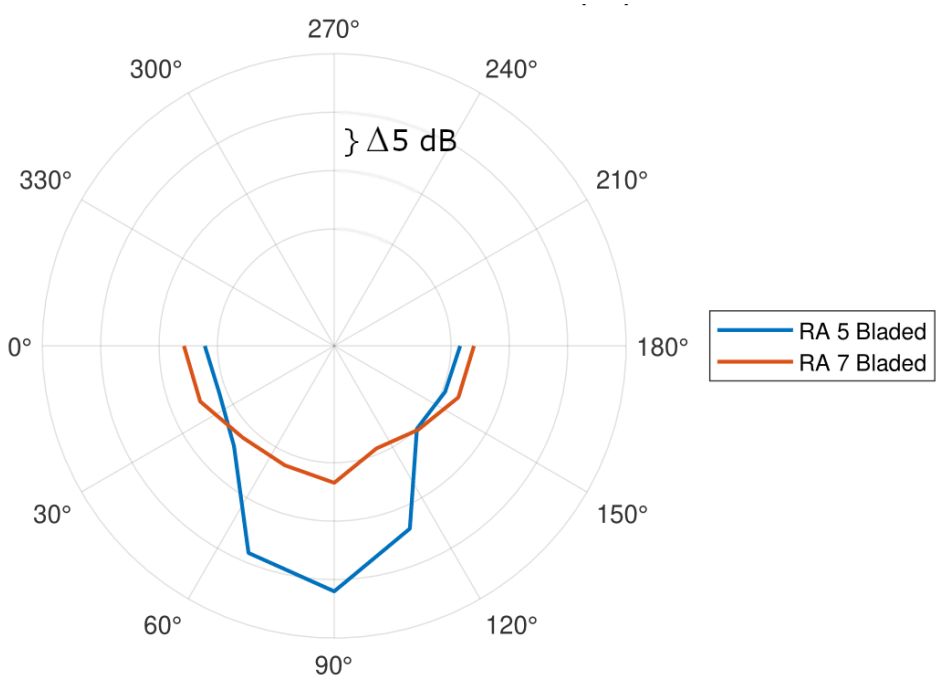

Figure 4.5: OASPL Noise contour (dB) for propellers RA and RA-7

The modeled results of blade count agree with studies concluding that increased blade count resulted in decreased overall noise. Hicks and Hubbard's same study found that an increase in chord-wise loading caused less severe increases in noise compared to increases in diameter. They concluded that any loss in thrust from diameter reduction could be regained by increasing blade area without additional noise penalties [29]. Moshkov and Samokhin further developed this blade area correlation to that of blade number by reducing a propeller's activity factor. Activity factor was defined as the power absorbed by an individual propeller blade. They experimentally found that a 9 dB reduction in noise could be achieved for the same aerodynamic loads switching from 2 to 3 blades. [28]. The modeled results of RA-7 in this study show similar noise patterns with changes in blade loading. Figure 4.6 shows that a decrease in activity factor resulted in a decrease in the average modeled propeller noise.

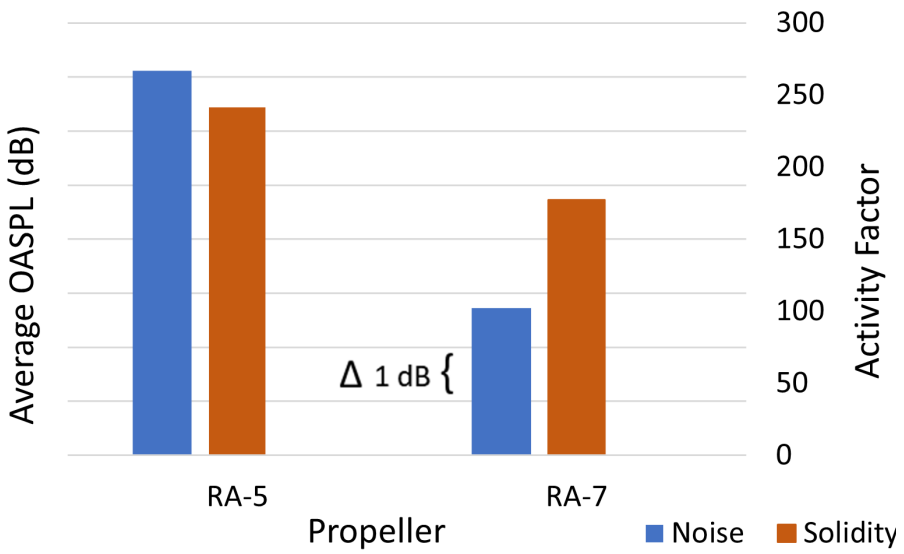

Figure 4.6: Change in average OASPL (dB) compared to activity factor for propellers RA and RA-7

Chapter 5

Flight Applications

The noise propagation module described in Section 2.3 is presented by assessing the noise characteristics of a multi propeller sub-scale STOL aircraft. Departure, cruise, and approach flight profiles were created using the aircraft's flap information and the propeller thrust as modeled in Section 2.1.1. Three assessments were then conducted on the sub-scale vehicle to demonstrate the methodology's capabilities of modeling community noise and to observe the noise effects of flight profile variation.

The first assessment explored component-based variations between propeller and airframe noise during overhead flight over a single observer in cases of takeoff, cruise, and approach. Flight profiles for all cases were generated based on the aircraft's specified drag and thrust requirements. Component and total noise were then propagated at takeoff and approach profiles across a community grid to explore directivity characteristics and the relative contribution of airframe and propeller noise to the total aircraft noise. Lastly, the sub-scale aircraft was modeled in the approach case with increasingly steep glide slopes to explore the effects changing flight profile have on community noise intensity and distribution over an area.

5.1 Flight Profile Creation and Source Noise Modeling

The profile analysis capabilities of the methodology described in Chapter 2 are presented through a preliminary assessment of an MIT sub-scale STOL vehicle equipped with eight propellers [30]. This sub-scale vehicle was chosen for assessment because of its available propeller geometry and flight performance characteristics [30]. Its STOL capabilities also allowed it to fly in a wide range of flight procedures. The following section describes a method of creating a flight profile given propeller performance characteristics and aircraft geometry. This analysis will focus on representative departure, cruise, and approach procedures shown conceptually in Fig. 5.1

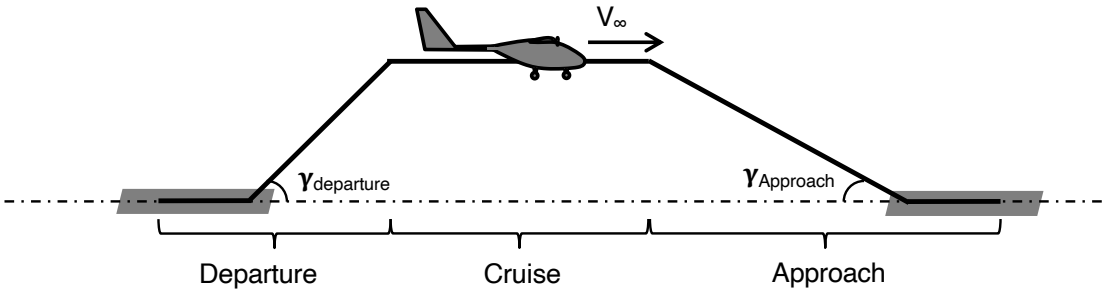

Figure 5.1: Baseline departure, cruise, and approach procedure representation for DP, blown flap vehicle noise modeling

The propeller throttle setting, flight velocity, flight path angle (γ), and flap setting for each operating condition are shown in Table 5.1. These parameters are used to generate a flight profile for each of the three conditions. The departure procedure assumed a full throttle setting and a constant flight path angle of 28° during the climb phase. Flight path angle and flight speed are based on estimated drag values, modeled in a previous study of the vehicle [31]. In a similar fashion, the cruise and approach flight profiles, described in Table 5.1, were based on flight speeds and flap settings used during steady cruise and a continuous descent approach procedure. For both cruise and approach, it was assumed that only the inner six propellers were operating [9].

Table 5.1: Baseline operating conditions for sub-scale DP, blown flap vehicle noise modeling

Operation	Throttle	Flight Speed (knots)	Flight Path Angle γ (°)	Flap Setting δ_f (°)
Departure	Full	18	28	25
Cruise	Full	63	0	0
Approach	50%	12	-8.9	40

The propeller source noise was modeled using the procedure described in Section 2.2. Forward velocity and travel direction were specified by the previously generated flight profile. The throttle position and flight speed were used to derive input RPM using the sub-scale's motor characteristics. Finally, the propeller airframe interaction noise was taken from a previous study operating the sub-scale aircraft in the same flight conditions [31]. Here, propeller wake-flap interaction noise was modeled using the Guo flap method [32] and wake-wing trailing edge interaction noise was modeled using the Fink method [33].

5.2 Aircraft Component Noise Modeling

The modeling method described in Section 2.3 is used to propagate noise from both propeller and airframe interaction sources to an observer located 50 feet directly underneath the aircraft. The A-weighted maximum sound pressure level noise ($L_{A,Max}$) for each of the three flight profiles described in 5.1, is shown in Figure 5.2 for the total propeller and airframe noise components.

5.2.1 Overflight Component Noise Propagation

Analysis of noise results indicated that the relative magnitude of each noise source with respect to one another are strongly correlated to operating condition. Propeller noise overpowers other component noise at nearly all phases, while the airframe noise contribution depends on the phase of flight. During departure and cruise, propeller noise was shown to

be over 10 dBA louder than airframe noise. It is only in the approach case where the airframe noise becomes closer in magnitude to the propeller noise. High airspeeds during the cruise phase resulted in higher propeller noise levels than in departure. Airframe noise is small due to the aircraft having flaps retracted during cruise.

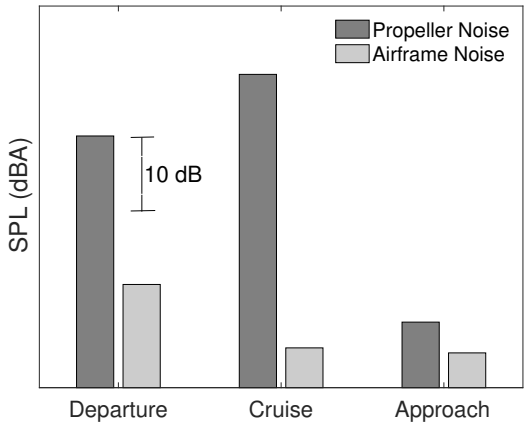

Figure 5.2: Modeled propeller and airframe noise levels of sub-scale STOL demonstrator at 50 feet overhead for different operating conditions, $L_{A,Max}$ (dB)

5.2.2 Community Component Noise Propagation

In addition to the single point overflight case, the community noise contours for the departure and approach procedures were also modeled. Figure 5.3 shows total sound exposure level (SEL) noise contours at low, medium, and high decibel levels, alongside the component noise breakdown during the STOL departure profile. The total noise (plotted in solid lines) was mainly comprised of propeller noise (plotted in dashed lines). This is especially clear at the low dB contour level (represented in black), where the airframe noise (plotted in dotted lines) accounted for less than 5 percent of area of both the propeller component noise and the total aircraft noise contours.

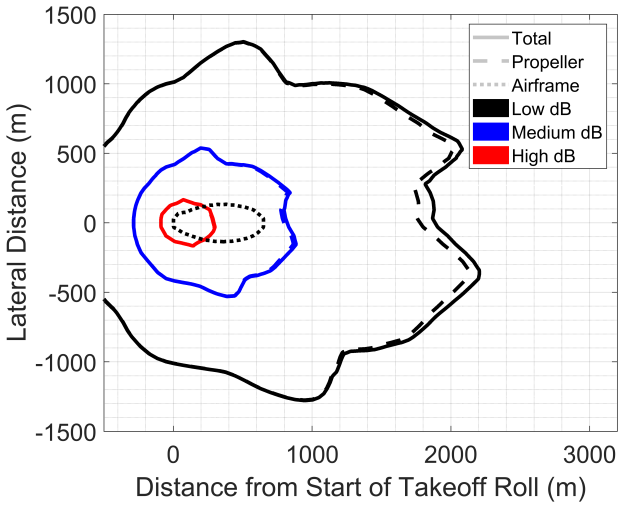

Figure 5.3: Modeled propeller and airframe noise contours of sub-scale STOL demonstrator in a 28° climb during departure, SEL levels each separated by 10 dB

The community noise results for the approach profile showing the modeled low, medium, and high dB contour levels, are shown in Figure 5.4. These results differ considerably from the departure profile. In the approach case, airframe noise (dotted lines) accounts for a larger portion of the total noise. At the low dB contour level, the airframe noise makes up a substantial 30 percent of the total noise. Even with such a high fraction of airframe noise, the total noise is mostly made of propeller noise, especially in medium and high decibel levels. The approach profile also had smaller and narrower contours than the departure case. At medium decibel levels, the approach contour is approximately 1000 x 200 m in area whereas the takeoff contour is about 2500 x 2200 m in area. These results indicate that in both takeoff and approach flight procedures, propeller noise is the main noise source for a STOL aircraft. Results suggest that airframe noise, though not the main contributor to total noise, has a potential impact on noise during landing.

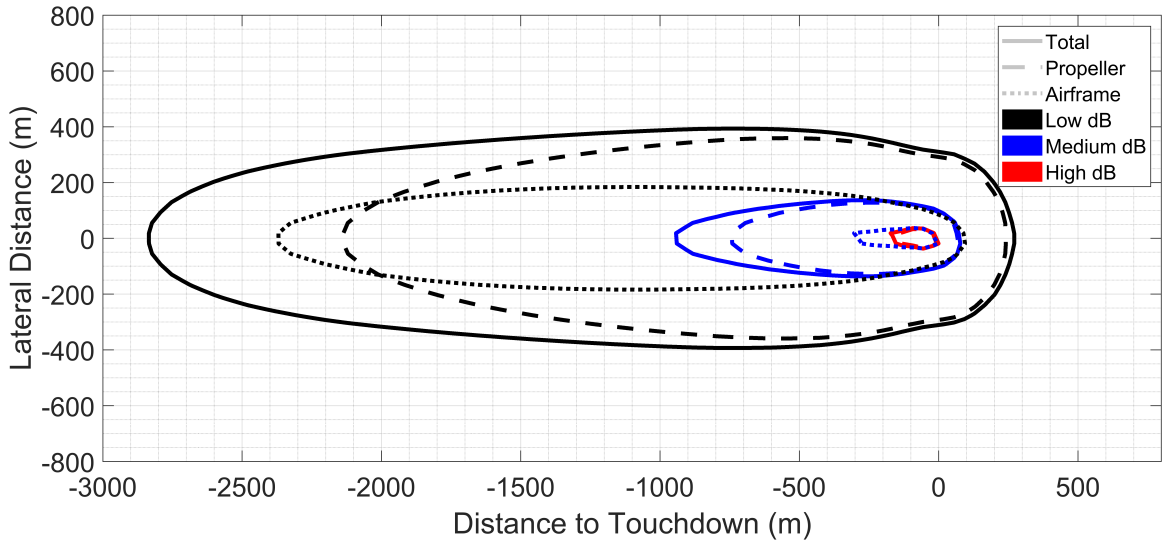

Figure 5.4: Modeled propeller and airframe noise contours of sub-scale STOL demonstrator in a -8.9° landing, SEL each separated by 10 dB

5.2.3 Analysis of Community Noise at Varied Approach Procedures

The flight profile methodology introduced in Section 5.1 presented three profiles for approach, cruise, and departure. For each of these profiles, however, various other flight path angles are possible though different combinations of thrust and flight velocities, as mentioned in Section 2.1.1. These variations in flight profile have the potential to change total community noise levels. The methodology's ability to capture such effects are demonstrated though the following analysis of total noise variation for three different flight profiles during approach. Figure 5.5 conceptually diagrams possible glide slope angles during approach that vary the distance and time spent over a certain ground area. This is achieved through adjustments in flight speed, aircraft flap setting, and thrust for a specific descent angle.

Table 5.2 describes the three approach procedures considered. Two thrust levels are considered: a high-powered (50%) approach throttle case, and a low-powered (25%) approach throttle case. For each thrust setting, three different flight path angles and corresponding approach velocities were used to create three cases of increasingly steeper approach.

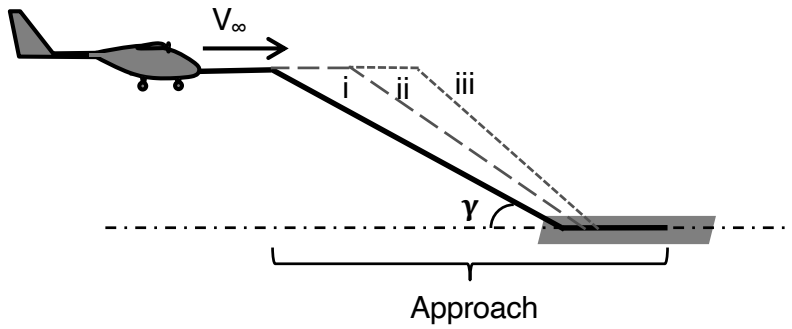

Figure 5.5: Representation of alternate approach procedures for DP, blown flap vehicle noise modeling

Table 5.2: Approach procedure operating conditions for sub-scale STOL noise modeling

Operation	Case	Throttle	Speed V_∞ (knots)	Path Angle γ (°)	Flap Setting δ_f (°)
High Power	i	50%	17	-3.1	40
Approach	ii	50%	12	-8.9	40
	iii	50%	10	-15.6	40
Low Power	i	25%	17	-6.9	40
Approach	ii	25%	12	-11.5	40
	iii	25%	10	-16.9	40

Figure 5.6 shows modeled SEL dB levels for the high-powered approaches at three different glide slopes with Path III being the steepest (solid lines). High and low dB levels, colored in red and black respectively, depict the relative magnitude of total noise across the community. The low and high level noise contours are 20 dB apart in magnitude. The contours become narrower and longer as the glide slope decreases. This is especially clear in the high decibel case, where Path III forms a curve 1500 m long and 900 m wide whereas the shallower Path I forms a longer and skinnier curve 2500 m long and 200 m wide. Under high-thrust levels, changes in glide slope affect noise contour shape, rather than its total area.

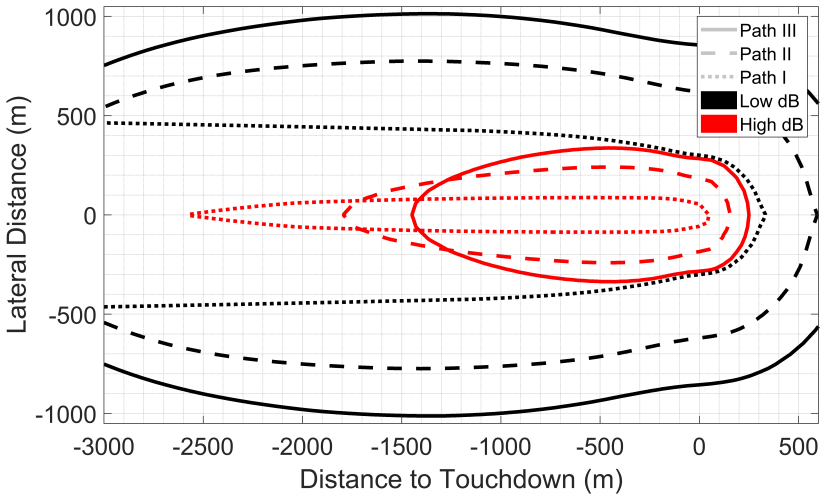

Figure 5.6: Modeled high-power approach noise contours of sub-scale STOL demonstrator, SEL levels each separated by 20 dB

This pattern becomes less defined in the low-powered approaches shown in Figure 5.7. As glide slopes steepen, they form noise ellipses of progressively smaller area, rather than contours that narrow and elongate like those of the high-thrust model. At low decibel levels, Path III forms a contour 500 x 200 m in area, while the shallower Path I forms a contour 1500 x 800 m in area. Compared to the high-thrust case, the low-thrust approach created smaller contours at all glide slopes. At low decibels, the low-powered contour is just over 250 m in length, whereas the high-powered case creates curves of over 2000 m in length. Adjusting the aircraft throttle during approach resulted in the largest change in total noise. Within each power setting, however, the results indicate a wide amount of different noise profiles exist when flight path angle is adjusted. Analysis showed that due to this breadth of noise profiles, certain flight paths cause a decisive reduction of total noise.

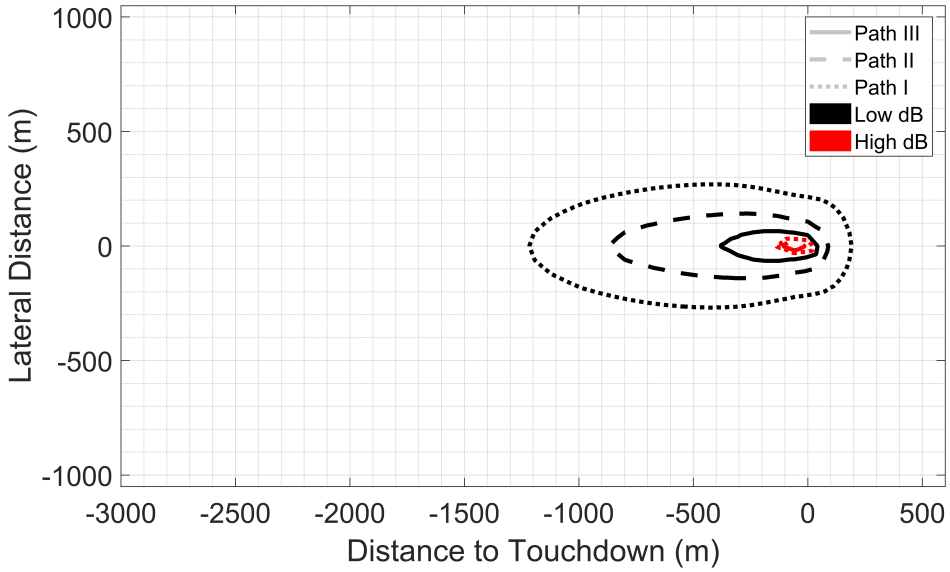

Figure 5.7: Modeled low-power approach noise contours of sub-scale STOL demonstrator, SEL levels each separated by 20 dB

Chapter 6

Conclusion and Future Studies

STOL and VTOL aircraft are topics of growing interest and application. They are especially well-suited for concepts such UAM, where their small takeoff and landing profile make them convenient for short flights in urban areas. Their application, however, nearly always involve multi propeller vehicles flying in close proximity to communities and areas of human habitation, where excessive levels of noise are a nuisance. This problem has motivated the development of a methodology to model and analyze multi propeller aircraft noise and the effects of flight procedure on community noise.

The methodology described in Chapter 2 models and propagates both broadband and tonal propeller noise. It has the capability to capture noise changes in the local scale of the propeller geometry and in the procedural scale by changing the flight profile. The methodology's modeled results were compared against noise measurements in Chapter 3. Close correlation was found between the modeled noise and the experimental measurements. Chapter 4 presented a case study which demonstrated the framework's ability to model noise caused by changes in propeller geometry though blade radius and propeller blade count. For the same power and RPM, reducing blade diameter and increasing propeller blade count resulted in decreased noise, which correlated with existing experimental studies. Chapter 5 demonstrated the methodology's ability to propagate component aircraft noise and model

community noise attenuation though changes in flight profile.

Although the methodology did not directly analyze airframe properties, aircraft source noise creation and noise propagation procedures can be readily applied to the current methodology to model total aircraft noise. For instance, the generated flight profile can also be used to specify aircraft flap and landing gear configuration which would create a more accurate community noise result. Although fixed wing, propeller driven aircraft were the focus of this methodology's applications, many other vehicles can be modeled using the same framework. Helicopter rotors can be modeled and analyzed by using non-uniform inflow models (described in Section 2.2.2) to account for leading rotor downwash and blade self-wake. Since the aircraft source noise module described in Section 2.2.2, has the capability to account for rotor tilt VTOL aircraft, such as tilt rotors and thrust vectored vehicles can be represented in this methodology. This allows more detailed analysis of vehicle-specific flight conditions, such as transition flight from vertical to forward flight. These additional capabilities of the noise methodology motivate further study in future work.

Bibliography

[1] Jordi Pons-Prats, Tanja Živojinović, and Jovana Kuljanin. On the understanding of the current status of urban air mobility development and its future prospects: Commuting in a flying vehicle as a new paradigm. *Transportation Research Part E: Logistics and Transportation Review*, 166:102868, 2022.

[2] Stephen A. Rizzi and et. al. Urban air mobility noise: Current practice, gaps, and recommendations. NASA TP–2020-5007433, 2020.

[3] Bolor-Erdene Zolbayar. Investigation of noise from electric, low-tip-speed aircraft propellers. M.s. thesis, The Pennsylvania State University The Graduate School College of Engineering, State College, PA, USA, 2018 [Online].

[4] National Air Traffic Services. Aircraft noise. Accessed Oct. 1, 2022 [Online].

[5] Jack E. Mad and Donald W. Kurt. A review of aerodynamic noise from propellers, rofors, and liff fans. Technical Report 32-7462, NATIONAL AERONAUTICS AND SPACE ADMINISTRATION, Langley Falls, VA, USA, 1970.

[6] Robert Dunn. What is sound pressure level (spl) and how is it measured? Pulsar Instruments, Oct. 15, 2019 [Online].

[7] Acoustic Glossary. Sound exposure terms and definitions. Accessed Nov. 18, 2022 [Online].

[8] NASA Preferred Reliablity Practices. Acoustic noise requirement. Technical Report PD-ED-1259, Jet Propulsion Laboratory, 1996 [Online].

[9] Siddhartha Krishnamurthy et al. Prediction-based auralization of a multirotor urban air mobility vehicle. In *AIAA Scitech 2021 Forum*, 2021 [Online].

[10] Mark Drela. QPROP Formulation. `https://web.mit.edu/drela/Public/web/qprop/qprop_theory.pdf`, 2006.

[11] Albert Betz. *Windenergie und ihre Ausnutzung durch Windmühlen*. Ökobuch Verlag, 1926.

[12] Sydney Goldstein. On the vortex theory of screw propellers. Royal Society, 1929.

[13] Theodore Theodorsen. *Theory of propellers*. McGraw-Hill Book Co., New York, 1948.

[14] S. Krishnamurthy, B. C. Tuttle, and S. Rizzi. A synthesis plug-in for steady and unsteady loading and thickness noise auralization. AIAA AVIATION 2020 FORUM, 2020.

[15] F. Farassat. A review of propeller discrete frequency noise prediction technology with emphasis on two current methods for time domain calculations. *Recent Advances in Aeroacoustics Springer-Verlag New York Inc.*, April 1986.

[16] Thomas F. Brooks, D. Stuart Pope, and Michael A. Marcolini. Airfoil self-noise and prediction. Technical Report 89-92, NASA, Langley Falls, VA, USA, 1989.

[17] Vít Štorcha et al. Measurement of noise and its correlation to performance and geometry of small aircraft propellers. In *EPJ Web of Conferences, Volume 114*, 2016 [Online].

[18] Robert T.N. Chen. A survey of nonuniform inflow models for rotorcraft flight dynamics and control applications. memorandum, NASA, Moffett Field, California, 94035, 1989 [Online].

[19] J. GORDON LEISHMAN. *Principles of Helicopter Aerodynamics*. CAMBRIDGE UNIVERSITY PRESS, 2000.

[20] Hermann Glauert. *The Elements of Aerofoil and Airscrew Theory*. Cambridge University Press, 1926.

[21] Robert P. Coleman et al. Evaluation of the induced-velocity field of an idealized helicoptor rotor. Report No. ADA801123, 1945.

[22] J. E. Ffowcs Williams and D. L. Hawkings. Sound generation by turbulence and surfaces in arbitrary motion. *Philosophical Transactions of the Royal Society*, 264(1151):321–342, May 1969.

[23] F. Farassat. Derivation of formulations 1 and 1a of farassat. Technical Report NASA/TM-2007-214853, Langley Research Center, Hampton, Virginia, USA, 2007.

[24] M. Kamruzzaman, Thorsten Lutz, K. Nuebler, and Ewald Krämer. Implementation and verification of an aeroacoustic wind turbine blade analysis tool. pages 8–10, 04 2011.

[25] Ze Feng Gan. Time-varying rotor noise computations and analysis of electric vertical take-off and landing aircraft. M.s. thesis, The Pennsylvania State University The Graduate School, University Park, PA, USA, 2021 [Online].

[26] C. F. Chien and W. Soroka. Sound propagation along an impedance plane. *Journal of Sound and Vibration*, 43(1):9–20, March 1975.

[27] Stephen A. Rizzi et al. A comparison of aircraft flyover auralizations by the aircraft noise simulation working group. In *AIAA AVIATION 2020 FORUM*, 2020 [Online].

[28] P. A. Moshkov and V. F. Samokhin. Evaluation of the influence of the number of blades and diameter on propeller noise. *VESTNIK of Samara University. Aerospace and Mechanical Engineering*, 15(3):25–34, 2016.

[29] Harvey H. Hubbard and Chester W. Hicks. Comparison of sound emission from two-blade, four-blade, and seven-blade propellers. Technical Report ADA801336, JET PROPULSION LABORATORY CALIFORNIA INSTITUTE OF TECHNOLOGY, Pasadena, CA, USA, 1947.

[30] C. Courtin, R. J. Hansman, and M. Drela. Flight test results of a subscale super-stol aircraft. AIAA 2020-0977, AIAA Scitech 2020 Forum, 2020.

[31] Nathan Yeung, Victoria R. Pellerito, Jessica De la Cruz, Melody Emmanouilidi, and Jacqueline L. Huynh. *Component-Based Noise Modeling for Distributed Propulsion Blown-Flap STOL Vehicle Flight Procedures*, chapter III, pages 9–12.

[32] Y. Guo. Aircraft flap side edge noise modeling and prediction. 32nd AIAA Aeroacoustics Conference, 2011.

[33] Martin Fink. Airframe Noise Prediction Method. Technical Report FAA-FRD-77-29, 1977.